Numerical analysis of scattered waves from rough surfaces with and without an object

Seung-Woo Lee, Akira Ishimaru, and Yasuo Kuga

Department of Electrical Engineering, University of Washington

ABSTRACT

The effects of rough surface scattering on the detection and imaging of objects are important in many applications including the imaging of objects on or near ocean surfaces and the detection of objects buried under ground rough surfaces. This paper focuses on the following problems: (1) Scattering from wedge-like rough surfaces representing ocean surfaces with sharp crested waves. (2) Scattering by objects above or below the rough surfaces. (3) UWB confocal imaging of objects near rough surfaces. Finite-Difference Time-Domain (FDTD) method is used to obtain frequency domain as well as time domain responses. Numerical simulations of various representative cases are conducted to understand and gain insight into the scattering effects on object detection and imaging.

Keywords: Rough surface scattering, Object detection and imaging, Finite-Difference Time-Domain method

1. INTRODUCTION

Electromagnetic/optical scattering from a rough surface or a random medium has attracted many researchers' interests because of its importance in various applications. One of the popular and challenging problems is the detection or imaging of the object which is embedded in the random medium or placed below or above the rough surface.

To achieve a successful tool for this problem, a good understanding of the scattering properties of the random medium with and without the object is essential. The stochastic properties of the random medium and the material property, shape and position of the object can generate diverse configurations. For this reason, numerical methods have been preferred because they can be applied for most cases without significant modification.

The two most commonly used numerical techniques for rough surface scattering problems are the Integral Equation Method (Moment Method) and the Finite-Difference Time-Domain (FDTD) method. While the integral equation method is more efficient for the Dirichlet surface scattering problem, the FDTD method is better suited for problems with inhomogeneous media and complex geometries including an object or discrete scatterers. The FDTD method was selected for our work, and with this method, time-domain responses as well as wide-band frequency-domain responses are available.[1]

In this paper, numerical simulations of a number of possible situations will be discussed, which include (a) scattering by wedge-like rough surfaces because of its importance in detecting objects in the presence of sharp crested ocean waves, (2) scattering effects of rough surfaces on the detection of objects located above or below ocean surfaces or rough terrains, (3) UWB confocal imaging of objects for possible application in the detection of buried objects. Numerical simulations are conducted to gain insight into the effects of rough ocean and terrain surfaces on the imaging and detection of objects.

Further author information: (Send correspondence to S.-W. Lee)
S.-W. Lee: E-mail: lsw@ee.washington.edu, Telephone: 1 206 543 2159, Address: Department of Electrical Engineering, University of Washington, 253 EE/CSE Building, Campus Box 352500, Seattle, WA 98195-2500 USA
A. Ishimaru: E-mail: ishimaru@ee.washington.edu, Telephone: 1 206 543 2169
Y. Kuga: E-mail: kuga@ee.washington.edu, Telephone: 1 206 543 0478

2. IMPLEMETATION OF FINITE-DIFFERENCE TIME-DOMAIN METHOD

The FDTD method is based on the differential forms of Ampere's and Faraday's laws. For the one-dimensional surface case, only E_z-, H_x-, and H_y-field (TM_z case) / H_z-,E_x-, and E_y-field (TE_z case) components are nonzero, and the corresponding Maxwell equations are given by,

$$\begin{aligned} \frac{\partial E_z}{\partial t} &= \frac{1}{\epsilon}\left(\frac{\partial H_y}{\partial x} - \frac{\partial H_x}{\partial y}\right) & \frac{\partial H_z}{\partial t} &= \frac{1}{\mu}\left(\frac{\partial E_y}{\partial x} - \frac{\partial E_x}{\partial y}\right) \\ \frac{\partial H_x}{\partial t} &= -\frac{1}{\mu}\frac{\partial E_z}{\partial y} & \frac{\partial E_x}{\partial t} &= \frac{1}{\epsilon}\frac{\partial H_z}{\partial y} \\ \frac{\partial H_y}{\partial t} &= \frac{1}{\mu}\frac{\partial E_z}{\partial x} & \frac{\partial E_y}{\partial t} &= -\frac{1}{\epsilon}\frac{\partial H_z}{\partial x} \end{aligned} \tag{1}$$

In our simulations, one-dimensional TM_z cases are considered.

Using Yee's central difference scheme in both time and space, we obtain for the TM_z case,[2]

$$\begin{aligned} E^{n+1}_{z(i,j)} &= E^{n}_{z(i,j)} + \frac{\Delta t}{\epsilon \Delta x}\left(H^{n+\frac{1}{2}}_{y(i,j)} - H^{n+\frac{1}{2}}_{y(i-1,j)} \right) \\ &\quad - \frac{\Delta t}{\epsilon \Delta y}\left(H^{n+\frac{1}{2}}_{x(i,j)} - H^{n+\frac{1}{2}}_{x(i,j-1)} \right) \\ H^{n+\frac{1}{2}}_{x(i,j+1)} &= H^{n-\frac{1}{2}}_{x(i,j)} - \frac{\Delta t}{\mu \Delta y}\left(E^{n}_{z(i,j)} - E^{n}_{z(i,j)} \right) \\ H^{n+\frac{1}{2}}_{y(i,j+1)} &= H^{n-\frac{1}{2}}_{y(i,j)} - \frac{\Delta t}{\mu \Delta x}\left(E^{n}_{z(i+1,j)} - E^{n}_{z(i,j)} \right) \end{aligned} \tag{2}$$

where Δ_x and Δ_y are spatial grids, and Δ_t is a time step. Note that electric and magnetic fields are positioned in a half step away from each other in both time and space. This enables every field variable in the current time step to be updated using the known values in the previous time step. The implementation for a three-dimensional problem is straightforward.

In applying the above update equations for the rough surface scattering problem, there have been several improvements made to the original FDTD method. The total field/scattered field formulation makes possible efficient implementation of plane wave or beam wave incidence, and near-to-far field transformation allows consideration of far-field scattering patterns as well as near-field interactions.[1] There have been many absorbing boundary conditions developed to efficiently reduce the computational domain. Among those, the Perfectly Matched Layer (PML) boundary condition[3] is most accurate, robust and widely applicable, although it requires more computational resources. Theoretically, the PML medium can absorb an impinging wave of any frequencies, at any angle, and from any media. But in practice, this can only be done by carefully choosing the parameters defining the PML medium, and sometimes it requires extensive numerical experiments. Particularly, in case of a highly elongated computational domain, special caution should be exercised because the incident angles onto the PML interface can be close to 90 degrees, and it is known that the performance of the PML degrades rapidly when an impinging angle goes to 90 degrees.

In order to overcome the inherent drawback of the FDTD method in handling a curved structure, a number of improved techniques have been proposed, which include the Conformal FDTD method, the Contour Path FDTD method, the Dielectric Subgrid Resolution technique, and the Non-orthogonal FDTD method, etc. It is obvious that using staircase modeling with the ordinary FDTD method is simplest and most efficient in terms of computational cost, but quite often it requires a too dense mesh to get an accurate result. To alleviate this burden, non-uniformly spaced grids or two (or more) different size grids can be used. The Conformal[5] and Contour Path FDTD methods use slightly modified updating equations near the curved interface with the help of the integral forms of Maxwell equations, so that the integral path is conformed to the rough interface. These methods need just a little more complicated routine and almost the same amount of memory and time compared to the staircase modeling. However, for some cases, they can cause so-called late time instability because in

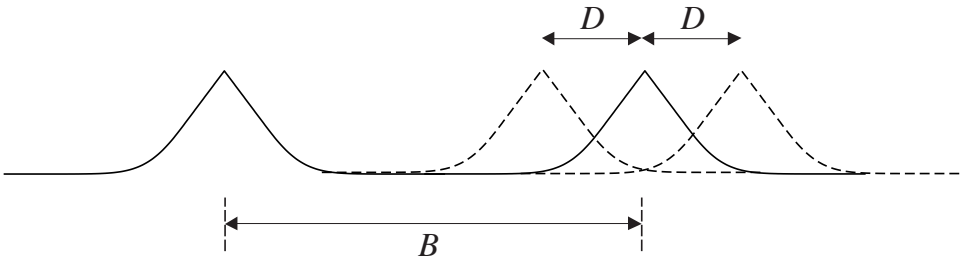

Figure 1. The average spacing is B (normalized to $\lambda = 1$), and the wedges are randomly distributed within $B \pm D$ where D is the elbowroom. The minimum spacing is $b = B - 2D$.

general the field values on the interface cannot be calculated explicitly, and they may require a much smaller time step size when the integral path is highly distorted.

In the Dielectric Subgrid Resolution technique[4] and other similar methods, the effective constitutive parameters are evaluated in a more clever way. Usually one cell is filled with a homogeneous medium, but in this method one cell is divided into four virtual sub-cells, and each sub-cell is filled with a properly averaged medium. Thus, the effective constitutive parameters are determined at the position of each field rather than inside each grid. Numerical experiments have shown that this technique has the effect of increasing grid resolution.

The non-orthogonal FDTD method is most complicated one and has been proved to be very reliable because it uses an arbitrarily shaped grid, so it can describe a given curved boundary more exactly. Every field in the non-orthogonal FDTD method has two different components and the updating of each field is made through the two step process. Contravariant components (located normal to each face) are updated first using the integral forms of updating equations which need the covariant fields in the previous step, and then covariant components (placed along each edge) are calculated using interpolation of contravariant fields in the neighborhood. As a result, this method requires almost the twice amount of memory and computation time. Since mesh quality is a critical factor determining the interpolation error and the time step size, a good mesh generation program is required. In this paper, the Conformal FDTD method and DSR technique are utilized for conducting and dielectric rough surfaces, respectively.

3. SCATTERING BY RANDOMLY DISTRIBUTED WEDGES

It has been noted[6] that sharp crested ocean waves may be acting as wedges, and the scattering from such surfaces may be important in low grazing angle (LGA) scattering. A detailed study of scattering by a single wedge-on-a-plane was conducted with special emphasis on the radius of curvature of the tip.[6] In this paper, we extend this study to wedges which are randomly placed on a flat surface with the average spacing B, the minimum spacing b, and the elbowroom D. The wedges are randomly distributed within $B \pm D$ with the average number of wedges per unit length designated by ρ. All quantities are normalized with the wavelength $\lambda = 1$ (Fig. 1).

Each wedge has the shape given by Browe et al.[6] For our study, we only considered the sharp wedges (radius of curvature $\rho_c \to 0$) (Fig. 2). The wedge shape is given by

$$\begin{aligned} y &= \sqrt{\frac{\alpha}{2}} h_m \left[-|x| + \sqrt{\frac{\alpha}{2}} \right] \qquad \text{for } |x| < \frac{1}{\sqrt{2\alpha}} \\ &= \frac{h_m}{2} e^{-\alpha x^2 + \frac{1}{2}} \qquad\qquad\quad \text{for } |x| > \frac{1}{\sqrt{2\alpha}} \end{aligned} \tag{3}$$

where $\alpha = \dfrac{1}{x_c^2}\left(\dfrac{5}{2} - \ln 2\right)$, and x_c is the effective length of the wedge. Note that at $x = x_c$, $y = h_m e^{-2}$. The wedges are placed without overlapping and, therefore, the following condition needs to be met.

$$B \;>\; 2D \;+\; 2x_c \tag{4}$$

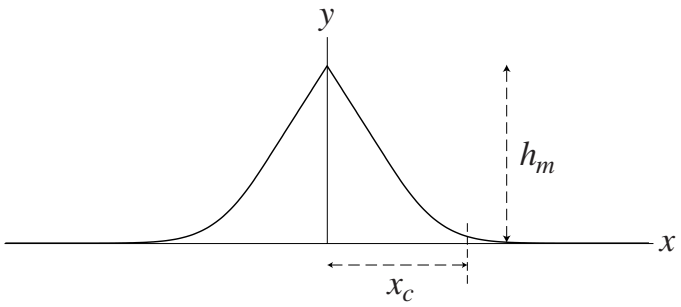

Figure 2. Geometry of a single wedge.

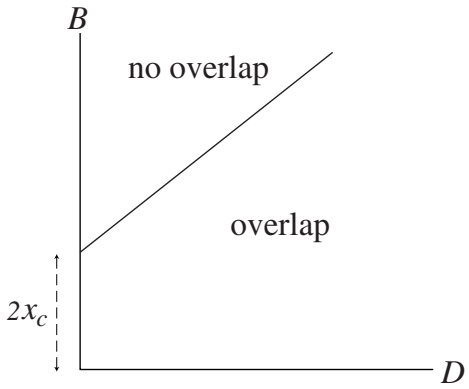

Figure 3. The spacing B, the elbowroom D, and x_c need to satisfy (2) to avoid overlapping.

This is pictured in Fig. 3.

3.1. Effects of the elbowroom D

Let us consider the numerical example with $h_m = 1\lambda$ and $x_c = 2\lambda$. Fig. 4 shows the normalized scattering cross section (NCSC) with an incident angle $\theta_i = 80°$ for $B = 12\lambda$ and five different elbowroom D. Note that in the back direction, the elbowroom D does not make much difference while in the forward direction, the larger D gives the more scattered power. The sharp peaks are grating lobes due to the average spacing B and given by

$$\sin\theta_g \;=\; \sin\theta_i \;\pm\; \frac{m}{B}, \quad m = \text{integer} \tag{5}$$

3.2. Effects of the wedge sizes

Next consider the different wedge sizes. Fig. 5 shows scattering patterns of the wedges with different heights and the same ratio of $h_m/x_c = 0.5$ which is considered by Browe et al.[6] Note that as the wedges size increases,

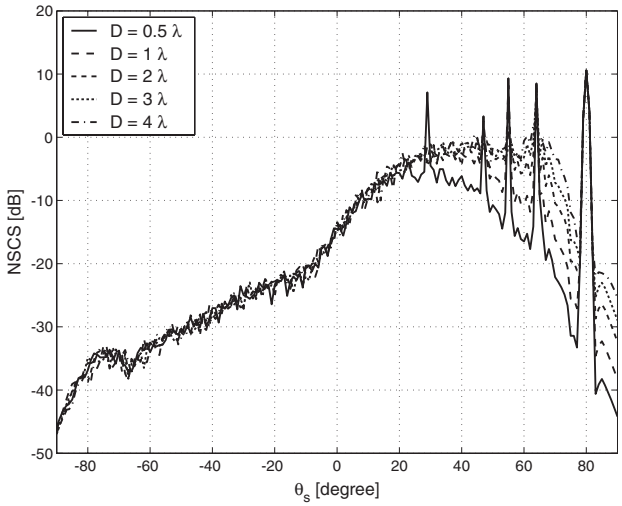

Figure 4. Normalized scattering cross section (NSCS) for different elbowroom. $B = 12\lambda, h_m = 1\lambda, x_c = 2\lambda, \theta_i = 80°$.

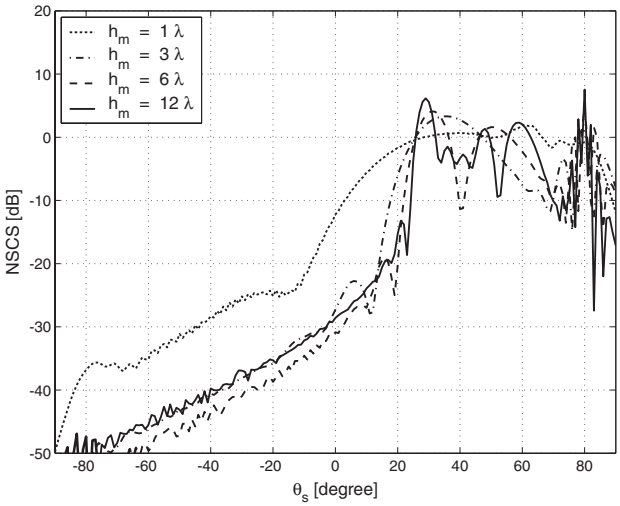

Figure 5. Effect of the wedge size. $h_m/x_c = 0.5, \theta_i = 80°$.

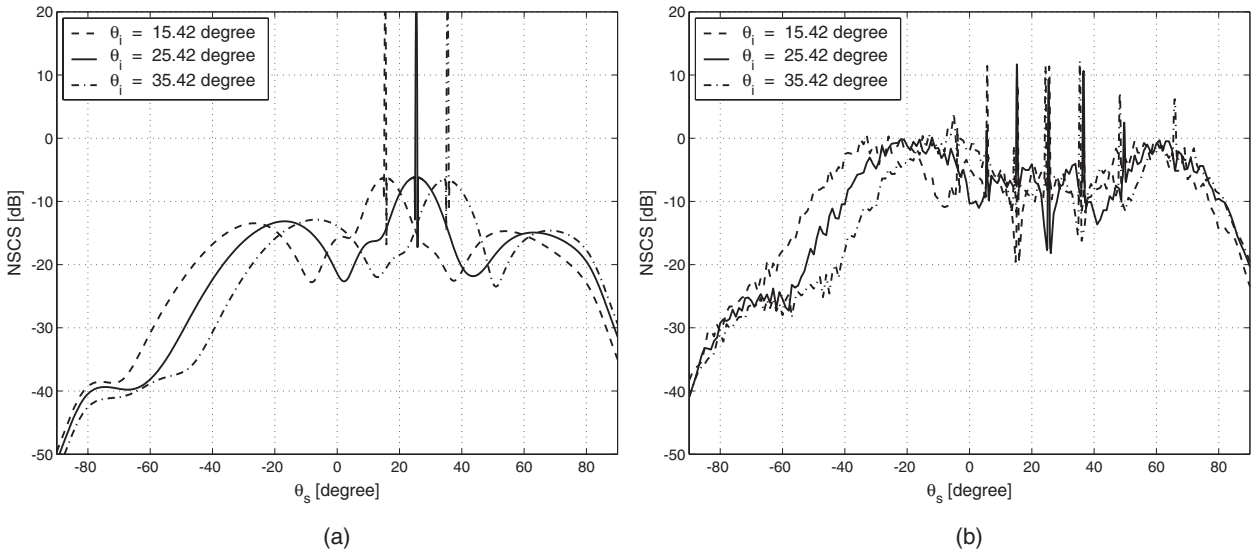

Figure 6. Scattering pattern for the different incident angles. (a) Single wedge. $h_m = 1\lambda, x_c = 2\lambda$ (b) Randomly distributed wedges. $B = 6\lambda, D = 1\lambda$.

the forward peak approaches to the specular angle of the wedge given by

$$\theta_{sp} \;=\; \theta_i \;+\; \theta_w \;-\; \pi \tag{6}$$

For our example, $\theta_w = 129.2°$ and, therefore, at $\theta_i = 80°$, we get $\theta_{sp} = 29.2°$. Note that for $h_m = 6$ which was considered in Ref. 6, the peak is clearly seen at 29.2°, but for smaller h_m, the peak gradually disappears.

3.3. Angles of incidence

Fig. 6(a) shows the scattering pattern for three different incident angles for a single wedge and Fig. 6(b) shows the scattering by distributed wedges. General shapes are similar, except the grating lobes due to the average spacings.

4. SCATTERING EFFECTS OF ROUGH SURFACES ON THE DETECTION OF OBJECTS

We consider an object below or above the rough surface (Fig. 7). The scattering pattern when the object is placed below the surface is shown in Fig. 8(a), which indicates the effects of the rms height h of rough surface.

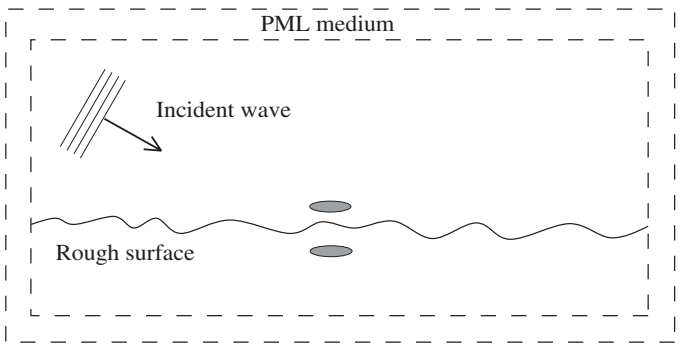

Figure 7. FDTD problem geomery for rough surface scattering with an object.

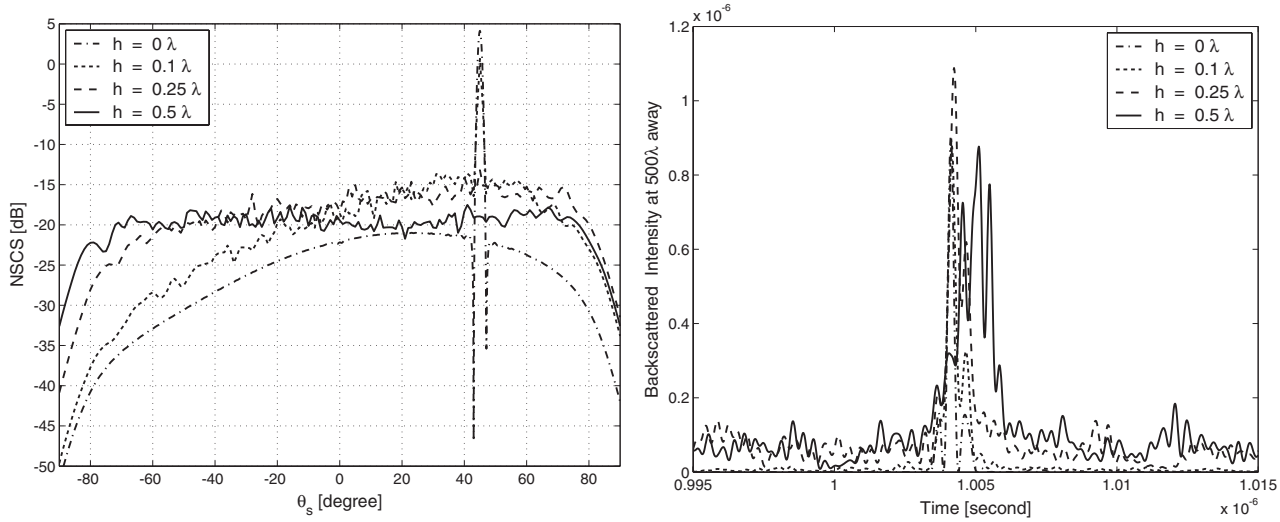

(a) (b)

Figure 8. Scattering by a PEC object embedded in a dielectric medium with a rough interface. $\theta_i = 45°$, correlation length $\ell = 0.5\lambda$, permittivity of the medium = 2, frequency = 1GHz. (a) Frequency domain (b) Time domain

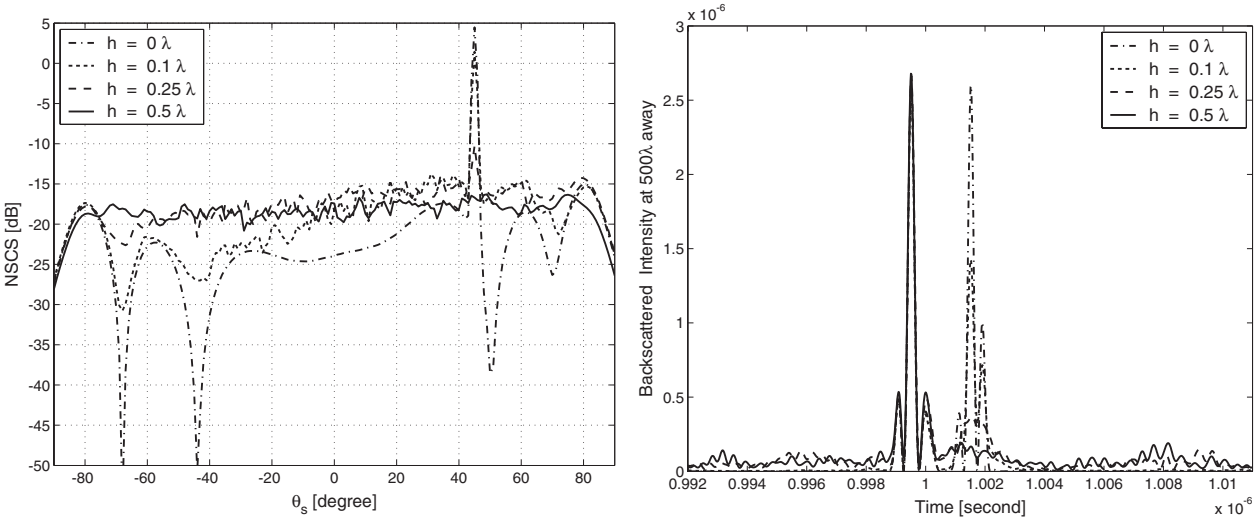

(a) (b)

Figure 9. Scattering by a PEC object placed over the rough surface. $\theta_i = 45°$, $\ell = 0.5\lambda$, permittivity of the medium = 2, frequency = 1GHz. (a) Frequency domain (b) Time domain

Note that the scattering from the object on a flat surface ($h = 0$) consists of the specular peak and scattering in other directions. As the rms height increases, the specular peak diminishes and the diffuse scattering is added to the non-specular scattering.

The scattering in time-domain is shown in Fig. 8(b). Note that as the rms height increases, the CW specular scattering diminishes, but in the time domain, the peak in time is visible even for the high rms heights indicating the usefulness of the time-domain detection of the object. The results for the case when the object is placed over the surface is shown in Fig. 9. In Fig 9(b), the first peak is due to the scattering from the object, and the second peak comes from the interaction between the object and the rough surface.

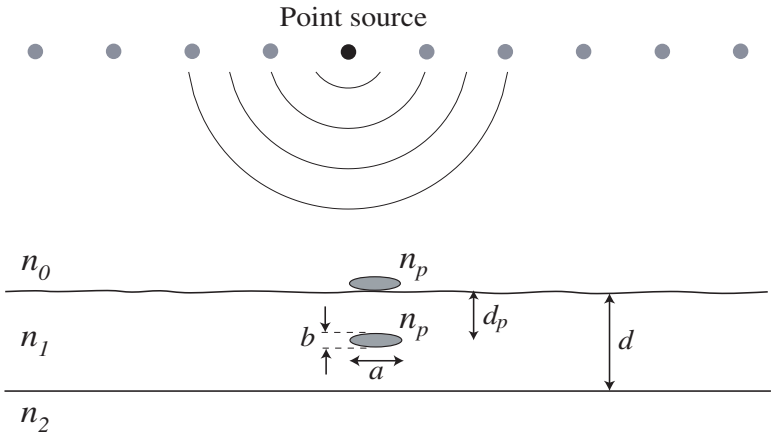

Figure 10. Geometry of UWB confocal imaging of an object. $n_0 = 1, n_1 = 1.46, n_2 = 4.123 - j0.048, n_p = 1.59 - j1.0$. $d = 1\mu m, d_p = 0.5\mu m$. $a = 0.6\mu m, b = 0.2\mu m$. $\lambda = 0.54\mu m$.

5. UWB CONFOCAL IMAGING OF OBJECTS NEAR A ROUGH INTERFACE

Confocal imaging of objects have been studied in the past.[9] We consider the imaging of objects near the dielectric material with roughness (Fig. 10). The technique used in this study is the same as given in Ref. 9 and UWB incident pulse is used to image the object. Fig. 11 shows the image of the object near the dielectric medium. Note that the use of the UWB pulse gives an excellent imaging resolution.

This method can be applied to detect contaminants and crystalline defects on the surface of silicon wafers using a near-field microscope.

6. CONCLUSIONS

In this paper, we focused on the scattering by randomly distributed wedges showing the effects of average spacing and elbowroom. Next, we considered the scattering by objects near the rough surface and showed the expected advantage of time-domain detection. Finally, we showed the superior imaging capability of UWB

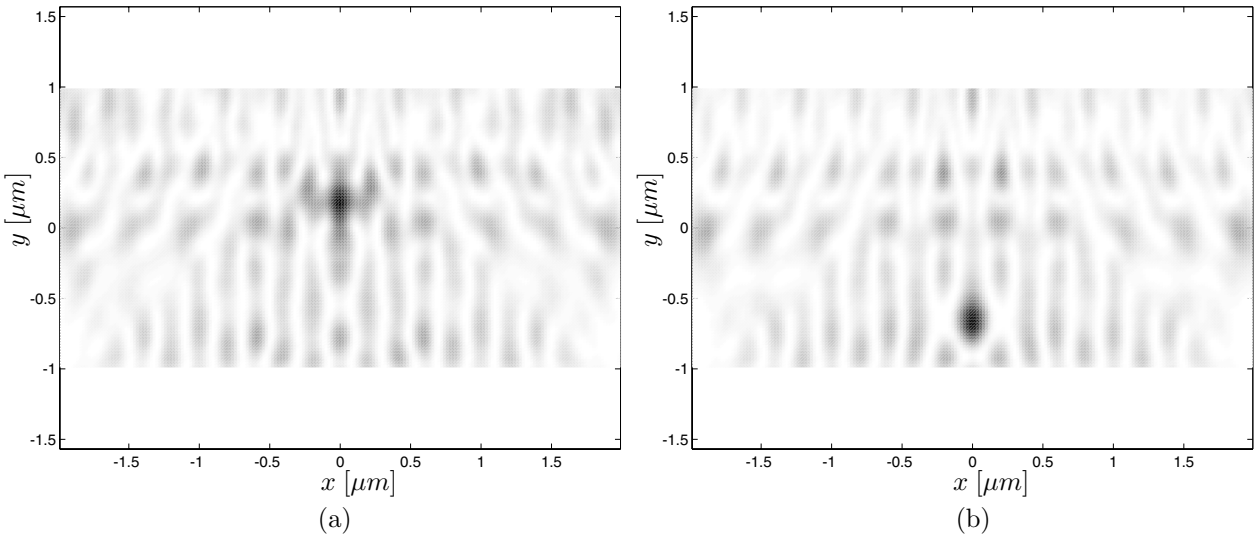

Figure 11. UWB confocal imaging of an object near the dielectric medium. (a) on the surface (b) below the surface

confocal imaging. These studies indicate the promising capabilities of these techniques for important practical problems of imaging of objects in the presence of complex environments such as rough terrain and general dielectric media.

ACKNOWLEDGMENTS

This work was supported by ONR(N000140010027) and NSF(ECS-9908849).

REFERENCES

1. A. Taflove and S. C. Hagness, *Computational Electrodynamics: The Finite-Difference Time-Domain Method*, 2nd ed. Boston, MA: Artech, 2000.
2. K. S. Yee, "Numerical solution of initial boundary value problems involving Maxwell's equations in isotropic media," *IEEE Trans. Antennas Propag.*, **14**, pp. 302–307, 1966.
3. J. P. Berenger, "A perfectly matched layer for the absorption of electromagnetic waves," *J. Comp. Phys.*, **114**, pp. 185–200, 1994.
4. G. Marrocco, M. Sabbadini, and F. Bardati, "FDTD Improvement by Dielectric Subgrid Resolution," *IEEE Trans. Microwave Theoy Tech.*, **46**, pp. 2166–2169, 1998.
5. S. Dey and R. Mittra, "A locally conformal finite-difference time-domain (FDTD) algorithm for modeling three-dimensional perfectly conducting objects," *IEEE Microwave Guided Wave Lett.*, **7**, pp. 273–275, 1997.
6. B. Browe, B. Davis, R. Adams, and G. Brown, "Scattering by a wedge-on-a-plane with a variable radius of curvature tip using the method of ordered multiple interactions," *RTO MP-60*, pp. 33-1–33-12, 2000.
7. X. Zhu and L. Carin, "Multiresolution time-domain analysis of plane-wave scattering from general three-dimensional surface and subsurface dielectric targets ," *IEEE Trans. Antennas Propag.*, **49**, pp. 1568–1578, 2001.
8. T. Dogaru, L. Collins, and L. Carin, "Optimal time-domain detection of a deterministic target buried under a randomly rough interface," *IEEE Trans. Antennas Propag.*, **49**, pp. 313–326, 2001.
9. A. Ishimaru, T.-K. Chan, and Y. Kuga, "An imaging technique using confocal circular synthetic aperture radar," *IEEE Trans. Geosci. Remote Sensing*, **36**, pp. 1524–1530, 1998.